Electronic Supplementary Material (ESI) for Nanoscale.

Supporting Information

The Interfacing Structure Effect of Ag/Graphene Oxide Nanohybrid Structures on Surface Enhanced Raman Scattering

Young-Kwan Kim,[a*] Gyeongsik Ok,[b] Sung-Wook Choi,[b] Hongje Jang[c] and Dal-Hee Min[d*]

[a] Carbon Composite Materials Research Center, Institute of Advanced Composite Materials, San 101, Eunha-ri, Bongdong-eup, Wanju-gun, Jeollabuk-do, 565-905 Korea

[b] Food Safety Research Group, Korea Food Research Institute, Backhyun 516, Sungnam, Gyeonggi-do 463-746, Korea.

[c] Department of Chemistry, Kwangwoon University, 20, Gwangwoon-ro, Nowon-gu, Seoul 139-701, Korea

[d] Center for RNA Research, Institute for Basic Science, Department of Chemistry, Seoul National University, Seoul, 151-747, Korea

**e-mail: youngkwan@kist.re.kr, Dr. Young-Kwan Kim, Fax:+82-63-219-8239, Tel:+82-63-219-8172*

**e-mail: dalheemin@snu.ac.kr, Prof. Dal-Hee Min, Fax:+82-2-889-1568, Tel:+82-02-880-4338*

Materials and Method

Synthesis of graphite oxide. GO was synthesized by modified Hummers method. 0.5 g of natural graphite and 0.5 g of $NaNO_3$ was added to 23 mL of H_2SO_4 with stirring in an ice bath. Then, 3 g of $KMnO_4$ was gradually added and the mixture was heated to 35 °C with stirring for an hour. Next, 40 mL of distilled water was slowly added and the mixture was heated to 90 °C with stirring for 30 min. The mixture was further diluted by addition of 100 mL of water. Finally, the 3 mL of H_2O_2 (30 % in water) was added dropwide with the color change of the solution from the dark brown to yellow. The synthesized graphene oxide solution was filtered with a Büchner funnel and washed with copious water until the filtrate was neutralized. The filter cake was dried under vacuum.

Synthesis of Ag NPs. 0.5 mL of 59 mM $AgNO_3$ and 1 mL of 34 mM sodium citrate aqueous solutions were added to 98 mL of water and this solution was stirred for 3 min. 0.5 mL of an aqueous 20 mM $NaBH_4$ solution, which had been aged for 2 h, was added all at once to the solution. The resultant solution was stirred for 1 h and aged for at least 24 h at room temperature before use. This suspension was used as a seed for Ag nanoplate synthesis and for preparation of AgNP/PAA-Si, GO and -RGO films.

Synthesis of Ag nanoplates. Two solutions (1 and 2) were prepared. Solution 1 was prepared by adding 900 μL of aqueous 40 mM hydrated hydrazine, 300 μL of aqueous 40 mM trisodium citrate, and 100 μL of AgNP suspension to 60 mL of water. On the other hand, Solution 2 was prepared by adding 300 μL of aqueous 59 mM $AgNO_3$ solution to 30 mL of aqueous solution. Next, solution 2 was (1 mL/min) added to solution 1 dropwise under strong stirring. After the addition, the solution was stirred for 30 min and brought to boil for 3-4 min to prevent further undesired changes of Ag nanoplates.

Supporting figures

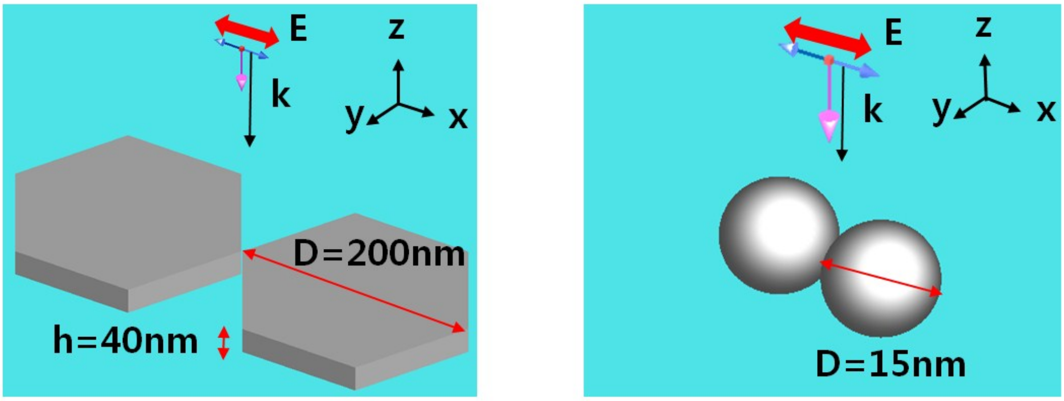

Figure S1. Perspective view of the 3D FDTD model (Left: Ag hexagonal plates, D=200nm, height=40nm; Right: Ag NPs, D=15nm). The x-polarized plane wave (514 nm wavelength) was used along the z-axis, illustrated in the perspective view of the model. The spatial resolution of the mesh override region was set to 0.2 nm for x-z direction and 0.5 nm for y-direction. The simulation time in all calculations was set to 500 fs. The refractive indices of dielectric layers such as APTES and PAA were 1.4, and the thicknesses of those layers were 1nm and 0.88nm, respectively. The refractive indices of GO and RGO were obtained from the ellipsometrical characterization results.[1] Finally, the refractive indices of Ag and Si were taken from E. Palik.[2]

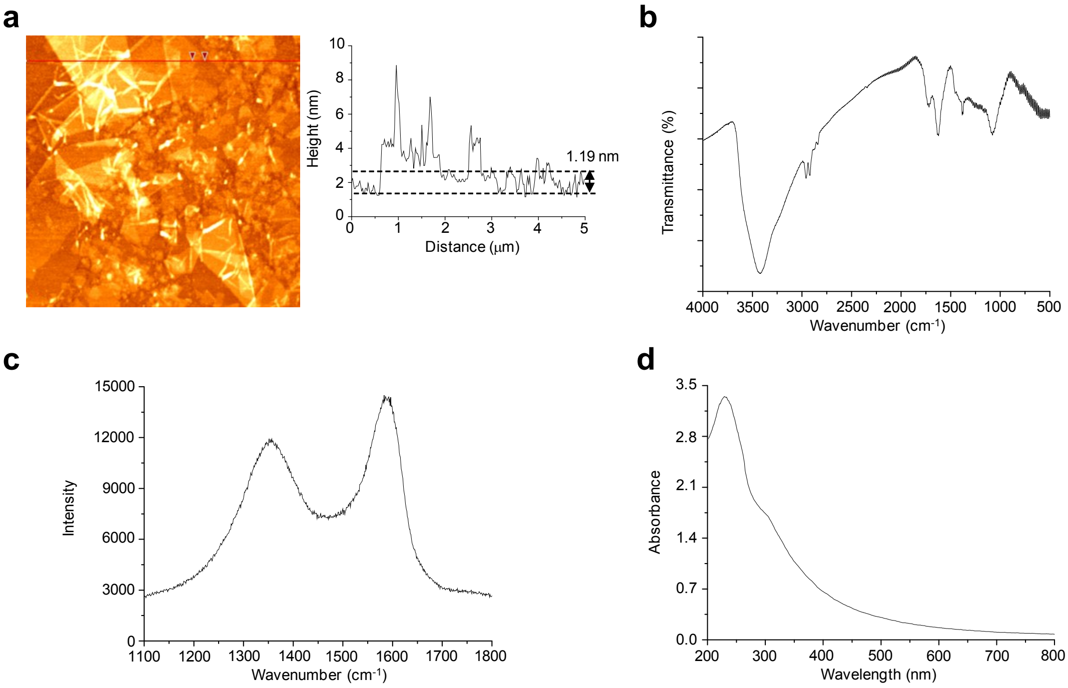

Figure S2. **Characterization of GO. a,** An AFM image and Line profile of GO films formed on Si substrates, which show the successful exfoliation of graphite oxide and high coverage immobilization of GO sheets. **b,** FT-IR spectrum of GO showed several characteristic peaks of oxygen-containing functional groups at 3415 cm^{-1} (O-H vibration), 1716 cm^{-1} (C=O stretching), 1627 cm^{-1} (C=C skeletal vibration of the oxidized graphitic structure), 1400 cm^{-1} (O-H deformation) and 1079 cm^{-1} (C-O stretching). **c,** Raman spectrum of GO showed typical D- and G- band at 1349 and 1611 cm^{-1} originated from defect structures of GO and graphitic structure of GO. **d,** UV-vis spectrum also showed typical absorption peak at 230 nm from π-π^* transition of aromatic C-C bond.

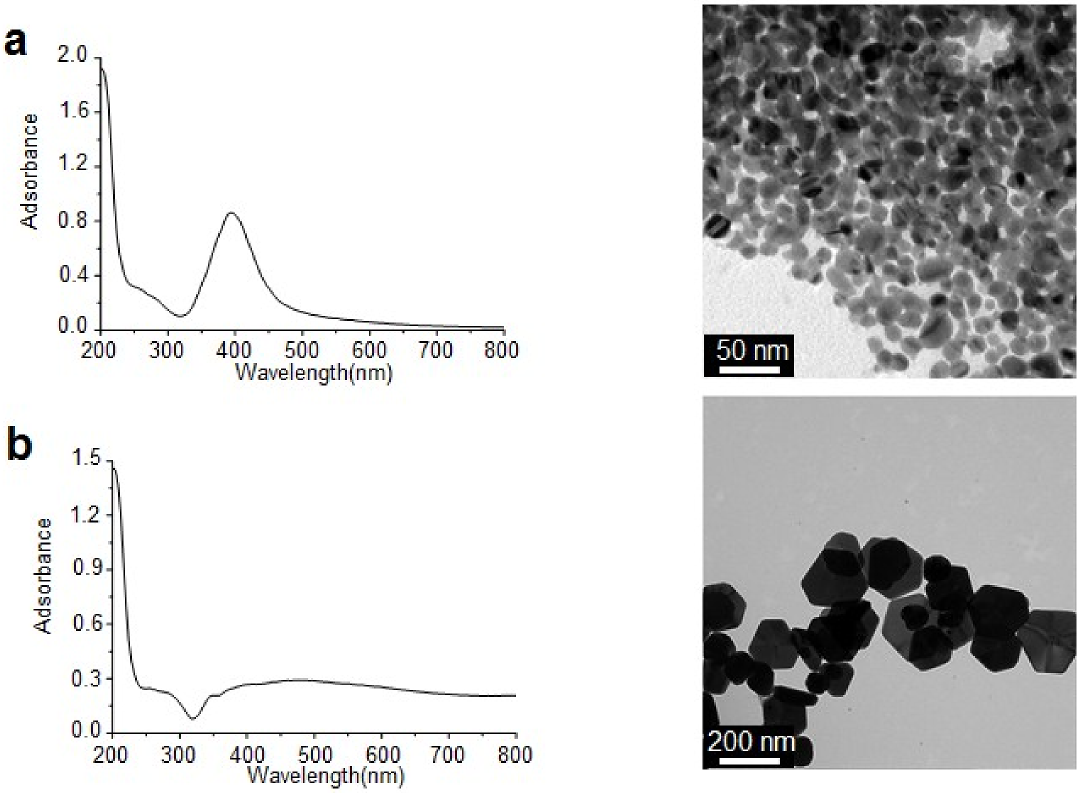

Figure S3. UV-vis spectra and TEM images of Ag NPs and Ag nanoplate. a, UV-vis spectrum and TEM image of Ag NPs respectively showed typical surface Plasmon resonance band at around 390 nm and 15 ± 5 nm in diameter. **b,** UV-vis spectrum and TEM image of Ag nanoplate respectively showed broad absorption in overall range of visible range because of its anisotropic structures and size distribution from 100 to 200 nm in edge length.

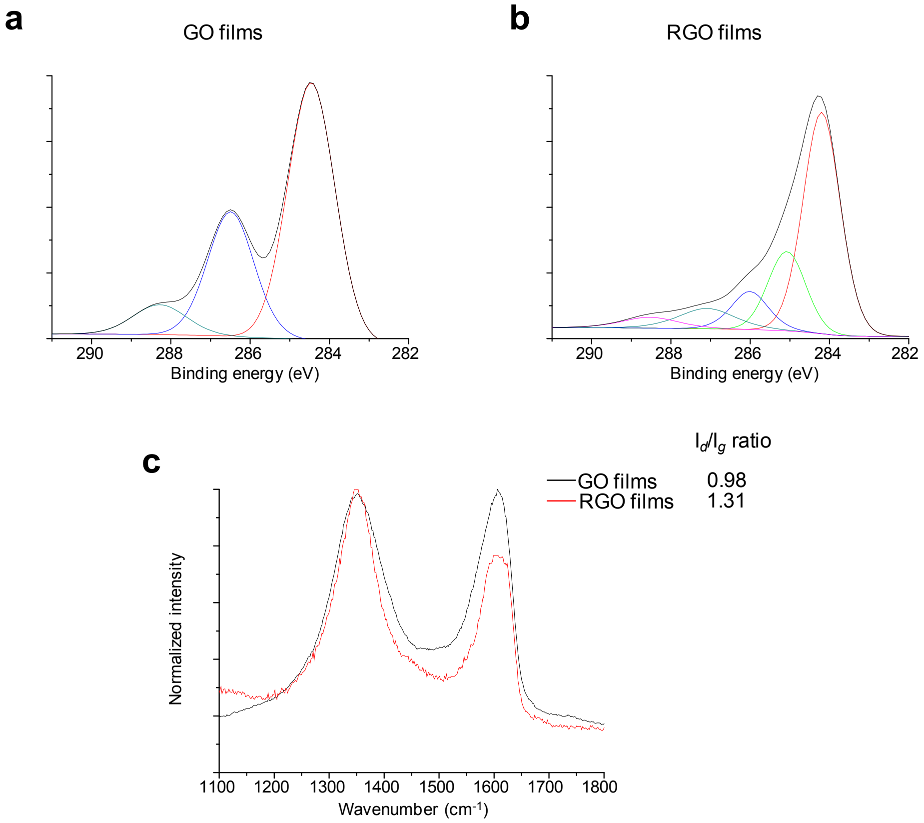

Figure S4. The XPS spectra of C1s and Raman spectra of GO and RGO films showed the successful reduction of GO films by hydrazine treatment. a, XPS spectra C1s of GO films showed typical C1s peaks at 284.5, 287.8, and 289.0 eV from graphitic structure, C-O and O-C=O bonds, respectively. **b,** After reduction, the peak intensities from oxygen-containing functional groups were weakened, which indicated the successful reduction of GO films by chemical reduction. **c,** Raman of GO and RGO films showed typical D- and G-peak at around 1350 and 1610 cm^{-1} and the relative intensity ratio of D- and G-peak intensity (I_d/I_g) of GO was increased by chemical reduction because of the newly formed small sized sp^2 carbon domains. Those results clearly confirmed the successful reduction of GO films by chemical process.

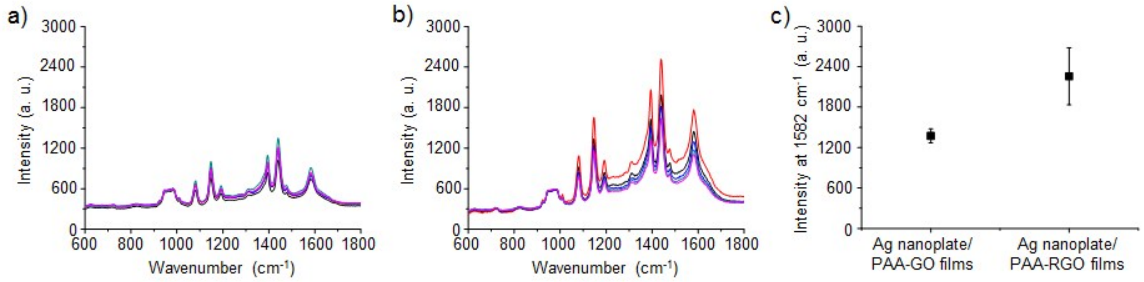

Figure S5. SERS spectra of 4-ATP on Ag NPs/PAA-GO (a) and Ag NPs/PAA-RGO films (b) obtained from 5 different measurement positions. Average SERS signal intensities of 4-ATP at 1582 cm^{-1} on Ag NPs/PAA-GO and Ag NPs/PAA-RGO films (c).

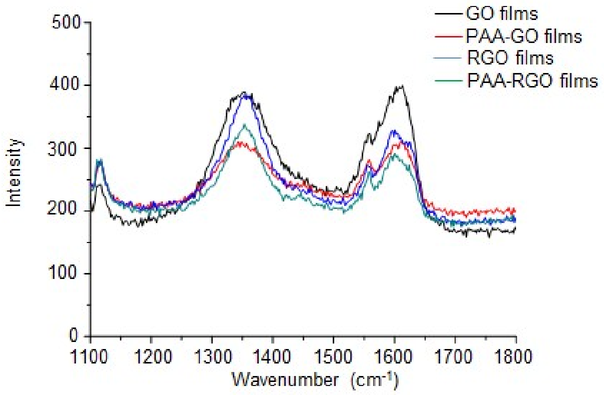

Figure S6. GO, PAA-GO, RGO and PAA-RGO films showed almost no SERS effect on 4-ATP. Raman spectra of GO, PAA-GO, RGO and PAA-RGO films which were incubated in 1 mM ethanolic solution of 4-ATP for 12 h showed almost no SERS signal of 4-ATP. Although there were two shoulder peak at 1100 and 1557 cm^{-1}, which can be assigned as b_2 mode of 4-ATP, the intensity of two peaks was negligible compared to the typical Raman peak of GO and RGO films such as D- and G-peak. This result clearly confirmed that the SERS signal enhancement of 4-ATP on Ag nanostructure/PAA-GO and Ag nanostructure/PAA-RGO films was not induced by direct charge transfer from PAA-GO and PAA-RGO films underneath Ag nanostructures.

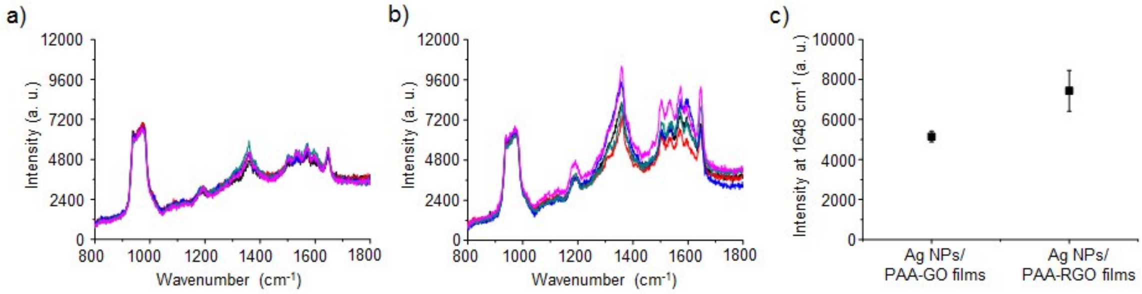

Figure S7. SERS spectra of R6G on Ag NPs/PAA-GO (a) and Ag NPs/PAA-RGO films (b) obtained from 5 different measurement positions. Average SERS signal intensities of R6G at 1648 cm^{-1} on Ag NPs/PAA-GO and Ag NPs/PAA-RGO films (c).

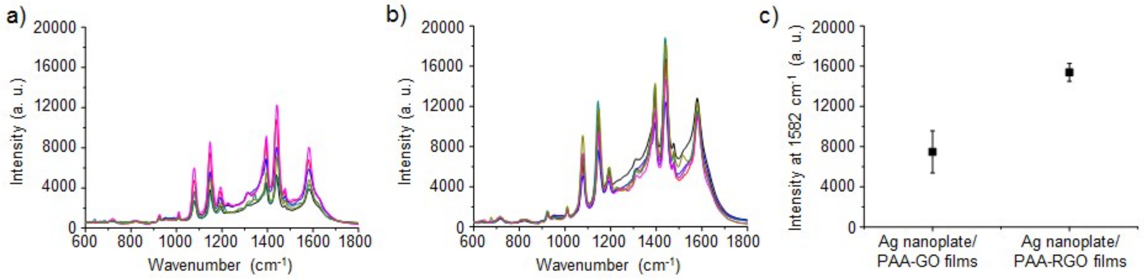

Figure S8. SERS spectra of 4-ATP on Ag nanoplate/PAA-GO (a) and Ag nanoplate/PAA-RGO films (b) obtained from 5 different measurement positions. Average SERS signal intensities of 4-ATP at 1582 cm^{-1} on Ag nanoplate/PAA-GO and Ag nanoplate/PAA-RGO films (c).

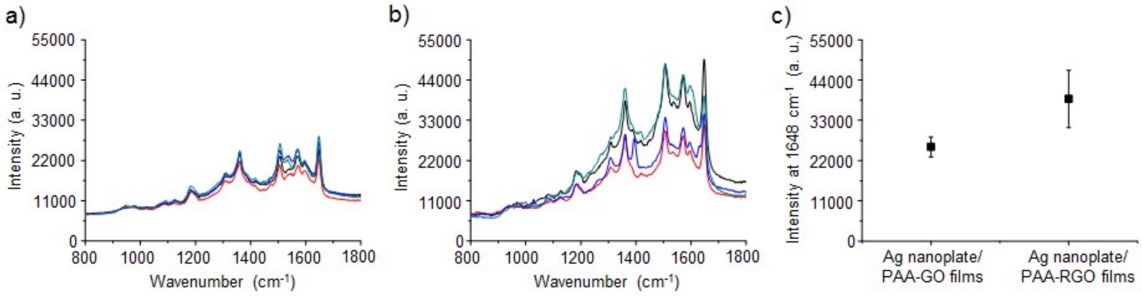

Figure S9. SERS spectra of R6G on Ag nanoplate/PAA-GO (a) and Ag nanoplate/PAA-RGO films (b) obtained from 5 different measurement positions. Average SERS signal intensities of R6G at 1648 cm^{-1} on Ag NPs/PAA-GO and Ag NPs/PAA-RGO films (c).

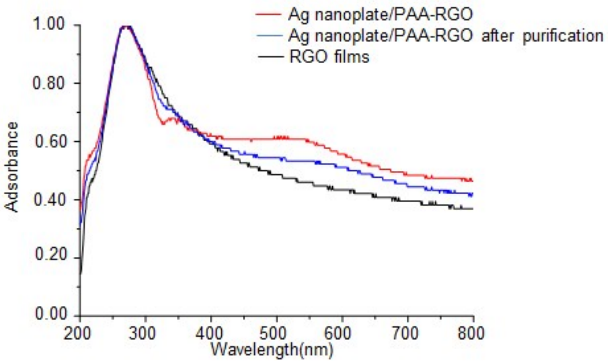

Figure S10. UV-vis spectra of RGO, Ag nanoplate/PAA-RGO and sonicated Ag nanoplate/PAA-RGO films. The RGO films showed red-shifted π-π* transition peak at 265 nm because of the newly formed sp^2 carbon domains by chemical reduction. After immobilization of Ag nanoplates on PAA-RGO films, the absorption in overall visible range increased with new peak around 550 nm by overlapping of absorption from Ag nanoplates. The peak around 550 nm was red-shifted by sonication because the removal of slightly aggregated and randomly oriented Ag nanoplates on PAA-RGO films. This result well agreed with the SEM result of Fig. 7a.

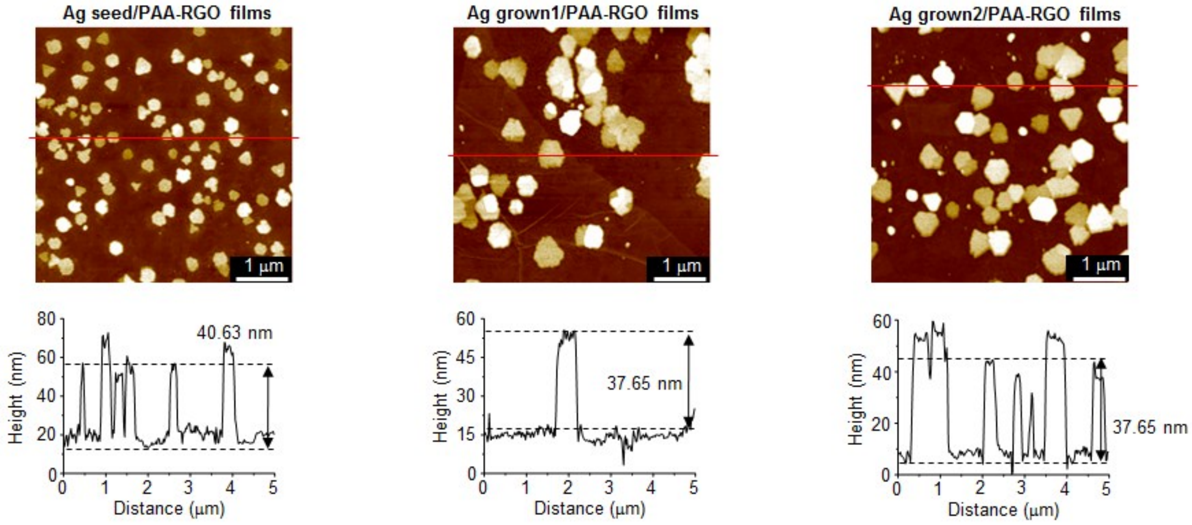

Figure S11. The successive lateral growth of Ag nanoplates on PAA-RGO films without change of their thickness. The thickness of Ag seed was around 40 nm and this value was not significantly changed during successive lateral growth.

References

1. I. Jung, M. Vaupel, M. Pelton, R. Piner, D. A. Dikin, S. Stankovich, J. An, R. S. Ruoff, *J. Phys. Chem. C* 2008, **112**, 8499.
2. E. D. Palik, Handbook of Optical Constants of Solids, Elsevier Inc. 1997.